MET.O.14

METEOROLOGICAL OFFICE
BOUNDARY LAYER RESEARCH BRANCH
TURBULENCE & DIFFUSION NOTE

T.D.N. No. 102

A SIMPLE CARTESIAN MODEL OF BOUNDARY LAYER FLOW OVER TOPOGRAPHY

By

P.J.Mason & R.I.Sykes

August 1977

FH1B

MASTER 25th August 1977

A SIMPLE CARTESIAN MODEL OF BOUNDARY LAYER FLOW OVER TOPOGRAPHY

P. J. Mason
and R. I. Sykes

Meteorological Office, Bracknell, U.K.

P 8, 11
Legend 9 & 4

16 pages and 6 figures

BOUNDARY LAYER FLOW OVER TOPOGRAPHY

Dr P.J.Mason,
Met.O.14,
Meteorological Office,
London Road, BRACKNELL,
Berkshire, U.K.

ABSTRACT

For circumstances under which it is practical to provide good resolution of a viscous boundary layer everywhere, a simple method for including no-slip, irregular boundaries into a Cartesian numerical model is presented. The method is a simplification of existing methods for dealing with irregular boundaries and is shown to the effective when the resolution requirements are satisfied.

1. Introduction

Recent interest in geophysical flows over topography has helped to stimulate research into numerical models of fluid flow over an irregular boundary. The importance of the general problem is obvious, since the geometry of the boundaries is one of the major determining factors in the flow field. In the atmospheric context, one feature worth noting is that the height of most topography is not very much larger than the boundary layer depth. So for atmospheric flows, the boundary layer will often play a crucial role in the dynamics.

The numerical problems involved in modelling irregular boundaries are serious, and a number of methods have been used to deal with them. The most obvious difficulty is that the boundaries do not generally coincide with coordinate surfaces in any convenient coordinate system. One method of removing this problem is to transform to a new coordinate system, which does contain the boundary as a coordinate surface. Gal-Chen and Somerville [1, 2] Thompson et al [3] describe the transformation of the Navier-Stokes equations into a general non-orthogonal coordinate system, and a numerical method of solving the equations. Other methods which allow an arbitrary disposition of grid-points, eg. the ICED-ALE method described by Hirt, Amsden, and Cook [4] and Pracht [5] , or finite-element techniques, can accomodate an irregular boundary without difficulty. In all these methods the equations become very complicated, especially in three dimensions, and the elliptic equation determining the pressure for an incompressible fluid is difficult to solve. As a result these models have slow execution speeds, which strictly limits the useful calculations that can be made.

To circumvent the problem of execution speed, some workers have attempted to include irregular boundaries in a Cartesian framework either by ensuring the boundary passes through grid-points, or by using Taylor series to extrapolate to the boundary. The first method is very crude, and only allows step-like boundaries, or straight ramps, whilst the second approach can lead to instability and loss of accuracy near the boundary, see Roache [6]. For an incompressible fluid, both methods require the solution of an elliptic equation for the pressure in an irregular domain. This usually necessitates the use of a point-relaxation iterative scheme, which is comparatively slow.

In this paper we describe a simple method of including topography in a Cartesian model of boundary layer flows, without changing the basic code. The method is developed by considering the topography as a region of arbitrarily high viscosity and density. The artifice of high viscosity and density is adopted to facilitate a simple analysis of how the equations can be solved in the entire rectangular domain. The method is an approximation to the Taylor series methods mentioned above [4, 5,6 7]. Viscous stresses only are made continuous across the boundary between the fluid and the topography. In order that these are the most important forces at the surface, a viscous boundary layer needs to be adequately resolved. The other terms in the equations are effectively evaluated with the step-like topography mentioned above. This limits the scales of topography which can be accurately dealt with to features not much larger than the boundary layer. For topography very much deeper than the boundary layer, methods such as the non-orthogonal coordinate system, ICED-ALE, or finite-element methods are necessary, especially since a lot of their complications are removed if the flow is effectively inviscid. Within the above limitation on the height of the irregularities, the method to be described gives a very efficient model of boundary layer flow over topography.

Details of the method are presented in the next section, followed by some results of integrations with various scales of topography in a rotating fluid. Although the model described here is two-dimensional, the method is just as easily incorporated into an existing three-dimensional model.

2. Numerical method and model

a. Basis of method

The basic system, illustrated in figure 1, is a no-slip, horizontal lower boundary, with a high viscosity fluid occupying the region below some specified surface S, and a low viscosity fluid above. The viscosity is a fixed function of space, and is not transported by the fluid. Obviously, in the limit as the viscosity below

the surface, $\nu_s \to \infty$, with the fluid viscosity ν_o fixed, the flow beneath the the surface will vanish, and the no-slip condition at the surface of the topography will be satisfied.

If the viscosities in a finite-difference model were set to either ν_o or ν_s depending on whether the grid-point was above or below S, then this would result in a step-like approximation to the surface. To improve on this, we need to consider which terms are important at the surface. Since we wish to achieve a no-slip condition on S, viscous stresses must dominate, therefore we enforce continuity of the viscous stresses $\rho \nu \left(\frac{\partial u_i}{\partial x_j} + \frac{\partial u_j}{\partial x_i} \right)$ across S. Note that the numerical model must resolve the boundary layer on S sufficiently accurately for the viscous terms to be dominant on the lowest grid-points above S.

We assume the density ρ is constant in what follows, and make $\nu \frac{\partial u_i}{\partial x_j}$ continuous across S by defining an interpolated viscosity on grid-points where a velocity gradient is calculated using velocities from both sides of the surface. The situation for the vertical gradient of the horizontal component of velocity, u , is shown in figure 2. The grid-points at which u is stored are denoted by crosses, and viscosities are required at intermediate points. Δ is the grid-length, which spans S, and η is the height of the surface above the lower grid-point, P. Suppose u_Q is the stored component at the upper grid-point Q, and similarly u_P . Then we can determine the velocity at the point R on the surface, u_R , by equating the stresses above and below S. Thus

$$\frac{\nu_o (u_Q - u_R)}{\Delta - \eta} = \frac{\nu_s (u_R - u_P)}{\eta} \qquad (2.1)$$

Solving for u_R gives the contribution to the stress as $\frac{\rho \nu_o \nu_s (u_Q - u_P)}{\nu_o \eta + \nu_s (\Delta - \eta)}$.
The model calculates the contribution $\int_0^{\infty} \frac{\rho \nu_{INT} (u_Q - u_P)}{\Delta}$,
thus

$$\nu_{INT} = \frac{\nu_o \nu_s \Delta}{\nu_o \eta + \nu_s (\Delta - \eta)} \qquad (2.2)$$

This procedure is equally applicable to horizontal derivatives, and results in a field of viscosity values which preserves viscous stresses across the surface.

Now it can be seen that the limit as $\nu_s \to \infty$ can be defined using relation (2.2). This gives interpolated values of viscosity as

$$\nu_{INT} = \frac{\nu_0 \Delta}{\Delta - \eta} \qquad (2.3)$$

Furthermore, since the solution for the flow beneath S is known in the limit $\nu_s \to \infty$, i.e. $u = v = w \equiv 0$, it is not necessary to use a numerical scheme capable of dealing with very large viscosities, and the velocities below S can be held fixed at these values for all time.

Provided a thermal boundary layer is also resolved, we can make conductive heat fluxes across the surface continuous in a precisely analagous manner. The conductivity of the hill may be taken as infinite if the hill is intended to be isothermal, and in this case the temperature is set equal to the chosen value at points beneath S. Arbitrary temperature profiles can be specified, but different temperatures need to be set depending on whether the grid-point value is being used to calculate a vertical or horizontal gradient.

To show that equation (2.3) is exactly the result which would be obtained by making a second order estimate of the second derivative at the point Q, we write a Taylor expansion around Q as follows:

$$u_T = u_Q + \Delta \left.\frac{\partial u}{\partial z}\right|_Q + \frac{\Delta^2}{2} \left.\frac{\partial^2 u}{\partial z^2}\right|_Q$$

$$u_R = u_Q - (\Delta - \eta) \left.\frac{\partial u}{\partial z}\right|_Q + \frac{(\Delta - \eta)^2}{2} \left.\frac{\partial^2 u}{\partial z^2}\right|_Q$$

Eliminating $\left.\frac{\partial u}{\partial z}\right|_Q$ from the above equations, a little algebra gives

$$\nu_0 \left.\frac{\partial^2 u}{\partial z^2}\right|_Q = \frac{\nu_0 \frac{u_T - u_Q}{\Delta} - \nu_0 \frac{u_Q}{\Delta - \eta}}{\Delta}$$

In the method described here the stress divergence $\frac{\partial}{\partial z}\left(\nu \frac{\partial u}{\partial z}\right)$ at the point Q is

$$\frac{\nu_0 \frac{u_T - u_Q}{\Delta} - \nu_{INT} \frac{u_Q - u_P}{\Delta}}{\Delta}$$

Thus when v_{INT} is given by equation (2.3) and Up = 0 this estimate is exactly the Taylor series estimate. (We are grateful to a reference for the above proof.)

This then is the essence of the method. Before describing the details of its incorporation into a particular finite-difference model we will discuss the magnitude of the truncation errors incurred near the surface.

Since our method requires the boundary layer thickness, δ, to be well resolved we consider a height z above the surface where $z \ll \delta$. The magnitude of the horizontal velocity component at z will be $u \sim \frac{U_0 z}{\delta}$, where U_0 is the free stream velocity. We only consider the horizontal momentum equations here, since errors in the vertical equation will be of the same order if the slope of the hill is O(1). In the case of very gentle topography, vertical accelerations are negligible, and the dominant error in the vertical velocity arises through the continuity equation.

Using the velocity scale U to estimate the terms in the horizontal momentum equation, (2.4 below) we obtain:

pressure and non-linear terms $\sim \frac{U_0^2 z^2}{\delta^2 L}$

Coriolis terms $\sim f U_0 z / \delta$

Viscous terms $\sim \nu_0 U_0 / \lambda \delta$

where L is the horizontal length scale and λ is the vertical scale of variation of the viscous stress near the surface. λ is obtained from a balance of terms in the momentum equation. The viscous term is dominant at the surface; whether it is balance by the inertial or Coriolis terms depends on the Rossby number $R = U_0 / fL$ For $R < 1$, it follows that $\lambda = \delta$, and for $R > 1$, $\lambda = (\nu_0 L \delta / U_0)^{1/3}$ is smaller than δ ie. for short length scales, an inner sublayer develops (cf triple-deck scale, Stewartson [7]).

At the surface our method calculates the viscous term to second order accuracy, but takes no account of the actual position of the surface in the calculation of the inertial and Coriolis terms. Thus the latter terms have a zero order relative error. However since these terms tend to zero at the surface, the errors are small in relation to the viscous scale, $\nu_0 U_0 / \Delta \delta$. For $R > 1$, the error in the inertial term relative to the viscous scale is $O(\Delta^2 / \lambda^2)$, and that in the Coriolis term is $O\left(\frac{\Delta}{\lambda} \cdot \left(\frac{\lambda}{\delta}\right)^2\right)$. For $R < 1$, the Coriolis term is always larger than the inertial term, and the error relative to the viscous scale is $O(\Delta / \delta)$. Thus the non-linear terms are effectively represented with second-order accuracy, but the Coriolis term has introduced first order errors which are only important for $R < 1$.

A similar analysis can be carried out for the buoyancy terms, assuming that these terms have a magnitude determined by the height of the topography, h, and the basic density gradient. This assumption should be valid when $U_0 / N h > 1$, where N is the Brunt-Väisälä frequency $\left[\frac{g}{\rho} \frac{\partial \rho_0}{\partial z}\right]^{\frac{1}{2}}$ (see § 3), and h is height of the topography. It follows that the ratio of resultant horizontal accelerations to the viscous stress gradien is $O\left(\frac{\Delta^2 h \lambda \delta N^3}{\nu_0 L U_0^2}\right)$. This is a second order error, and the extra length scale provided by th stratification is not restrictive for geophysical parameters. When $U_0 / N h < 1$, the buoyancy perturbations, and hence the errors, are smaller than the above estimates.

Finally, although our method has no integral mass flux errors, there are local errors in mass fluxes near the surface. Consider the horizontal flux across the interval PQ of figure 2. The horizontal velocity at Q will be $\alpha(\Delta - \eta)$, where α is the velocity gradient at the surface. Thus the flux is $\frac{\alpha}{2}(\Delta - \eta)^2 +$

third order terms. Since our method approximates the viscous terms to second order, the velocity at Q will be correct to second order in $(\Delta-\eta)$. Thus the implied flux across PQ is $\frac{\alpha}{2}\Delta(\Delta-\eta)$, giving a maximum error of $\frac{1}{8}\alpha\Delta^2$. These errors are worse than the $O(\Delta^3)$ errors in flux estimates away from the boundary and imply a first order transport across the surface. However, in practice the factor of $\frac{1}{8}$ (a factor of $\frac{1}{4}$ is essentially due to the accuracy of the viscous terms) means that unless the interior resolution is very fine these errors are not significantly larger than the second-order interior errors.

b. Numerical model

The method outlined above has been incorporated into a two-dimensional Cartesian model of an incompressible, Boussinesq fluid. The equations of motion to be solved are

$$\frac{\partial u}{\partial t} + u\frac{\partial u}{\partial x} + w\frac{\partial u}{\partial z} = -\frac{\partial p}{\partial x} + fv + \frac{\partial}{\partial x}\left(2\nu\frac{\partial u}{\partial x}\right) + \frac{\partial}{\partial z}\left(\nu\frac{\partial u}{\partial z} + \nu\frac{\partial w}{\partial x}\right) \qquad (2.4)$$

$$\frac{\partial v}{\partial t} + u\frac{\partial v}{\partial x} + w\frac{\partial v}{\partial z} = -\frac{dp_0}{dy} - fu + \frac{\partial}{\partial x}\left(\nu\frac{\partial v}{\partial x}\right) + \frac{\partial}{\partial z}\left(\nu\frac{\partial v}{\partial z}\right) \qquad (2.5)$$

$$\frac{\partial w}{\partial t} + u\frac{\partial w}{\partial x} + w\frac{\partial w}{\partial z} = -\frac{\partial p}{\partial z} - \frac{g\rho}{\bar{\rho}} + \frac{\partial}{\partial x}\left(\nu\frac{\partial w}{\partial x} + \nu\frac{\partial u}{\partial z}\right) + \frac{\partial}{\partial z}\left(2\nu\frac{\partial w}{\partial z}\right) \qquad (2.6)$$

$$\frac{\partial \rho}{\partial t} + u\frac{\partial \rho}{\partial x} + w\frac{\partial \rho}{\partial z} = \frac{\partial}{\partial x}\left(K\frac{\partial \rho}{\partial x}\right) + \frac{\partial}{\partial z}\left(K\frac{\partial \rho}{\partial z}\right) \qquad (2.7)$$

$$\frac{\partial u}{\partial x} + \frac{\partial w}{\partial z} = 0 \qquad (2.8)$$

where the coordinate axes and velocity components are as shown in figure 1.f is the Coriolis parameter, g is the acceleration due to gravity, $\bar{\rho}$ the mean density, ρ the perturbation density, ν the kinematic viscosity, and K the thermal diffusivity. The only term involving a derivative with respect to y is dp_0/dy, which is a constant and generates the basic geostrophic flow through the domain of integration.

Variables are stored on the standard staggered grid, eg Williams /8/, sketched in figure 3. The grid is uniform in the x-direction, and is stretched in the z-direction to resolve the boundary layer. Leapfrog time-differencing is used, and all spatial derivatives are centred, so the finite-differencing is second-order accurate in space and time. Owing to the well-known unconditional instability of the viscous

an explicit
terms with a leapfrog formulation, a du Fort-Frankel scheme is used for the viscous terms, i.e. the value at the grid-point under consideration is replaced by the average of the values at the advanced and the previous time-levels.

The inertial terms are calculated using the 'absolutely conserving' scheme of Piacsek and Williams [7]. This scheme conserves the total kinetic energy, apart from errors in the divergence. As we shall see below, the Poisson equation for pressure is solved by a direct method, and apart from machine truncation, the only errors in the divergence are due to the fact that the du Fort-Frankel terms need to be approximated in deriving the pressure. However, these errors are small provided the temporal evolution is on a timescale much longer than the timestep, and vanish in the steady state.

Periodic boundary conditions were specified in the x-direction, while at the lower boundary, $z = 0$, we specify $u = v = w = 0$ and at the top of the model, $z = H$, there is a stress-free, rigid lid, i.e. $\frac{\partial u}{\partial z} = \frac{\partial v}{\partial z} = w = 0$.

The boundary conditions on the elliptic equation for pressure are particularly simple in the Cartesian model, in contrast to the non-orthogonal coordinate model. The pressure equation is obtained by taking the finite-difference equivalent of the divergence of the momentum equations.

If we write the momentum equations (2.4) and (2.6) as

$$\frac{\partial \underset{\sim}{u}}{\partial t} = -\nabla p + \underset{\sim}{T} \qquad (2.9)$$

where $\underset{\sim}{u} \equiv (u, w)$, $\nabla \equiv \left(\frac{\partial}{\partial x}, \frac{\partial}{\partial z}\right)$ and $\underset{\sim}{T} \equiv (T_x, T_z)$ represent all terms other than the pressure gradient, then

$$\nabla^2 p = \nabla . \underset{\sim}{T} \qquad (2.10)$$

Equation (2.9) represents the equation for pressure in the finite-difference model, provided ∇ denotes a finite-difference operator, and then the right hand side is required at all interior grid-points.

The derivation of the Poisson equation (2.10) beneath S requires further discussion. In the limit $\nu_s \to \infty$, $\underset{\sim}{u} \equiv 0$ below S and provided we let the density $\bar{\rho} \to \infty$ below S the pressure forces are negligible. Thus the only diagnostic pressure equation which is consistent with the finite difference analogue of the continuit equation is obtained by setting $\underset{\sim}{T} = 0$ at all points beneath S, as can be seen from equation (2.9). This ensures that the continuity equation is satisfied on our mesh. but incurs the flux errors near the surface described in the previous section.

It will be seen that values of T_z outside the domain are required to define the right hand side of (2.10) at all interior points. Since w = 0 on both upper and lower boundaries, the boundary condition on pressure is

$$\frac{\partial \rho}{\partial z} = T_z \quad \text{on} \quad z = 0, H ,$$

and it can be shown that if this boundary condition is applied, then the solution for ρ at all interior points is independent of the value assigned to T_z outside the domain. The horizontal boundaries lie on the levels containing the w-points, see figure 3, so the pressure is only required at interior points to advance the fields. Hence we set $T_z = 0$ below z = 0 and above z = H, and solve the Poisson equation with boundary conditions $\frac{\partial \rho}{\partial z} = 0$ on z = 0, H. The equation is solved using a Fast Fourier Transform for the x-direction, and line inversion of the resulting tri-diagonal matrix for the z-direction.

We have found that the du Fort-Frankel scheme does <u>not</u> give unconditional stability of the viscous terms when Coriolis terms are also present. We have not presented our linear stability analysis because empirical results from our model indicated the importance of spatial variations in viscosity. (A similar stability analysis by Lipps [10] was brought to our attention by a referee). The empirical results show a rapidly oscillating instability when $\frac{\nu_{max} \Delta t}{\Delta z^2} >$ constant of order 1. Here Δt is the time-step, Δz is the smallest grid-length, and ν max is the maximum viscosity used by the model. This will be one of the interpolated viscosities, since viscosities beneath S are not used in the numerical scheme. This stability criterion limits the maximum viscosity which can be calculated from equation (2.3). However, the criterion is not very restrictive, since in most cases, limiting the interpolated viscosities to satisfy $\nu_{INT} \Delta t / \Delta z^2 < 0.5$ at each point effectively only changes the position of S by a small fraction of a grid length.

For flows in which $\frac{\nu_0 \Delta t}{\Delta z^2}$ is not much less than 0.5 (none of which are presented below), we have found that the use of larger interpolated viscosities, without instability, is made possible by the application of a time smoother to the u,v,w, and ϱ fields. The values of a field ϕ at time levels n and n-1, which are used in the leapfrog scheme to produce values at time n+1, are replaced by smoothed values ϕ_s^n and ϕ_s^{n-1}, defined by

$$\phi_s^n = (1-\varepsilon)\,\phi^n + \varepsilon\,\phi^{n-1}$$

$$\phi_s^{n-1} = (1-\varepsilon)\,\phi^{n-1} + \varepsilon\,\phi^n$$

where ε is about 0.05. The use of this time smoothing clearly does not affect steady state solutions, and comparison with unsmoothed results in cases where they were stable showed insignificant differences, apart from a reduction in timescale by a factor of $(1-\varepsilon)$.

Finally, the slow 'time-splitting' instability of the leapfrog scheme is removed by the use of an occasional forward timestep. This is only first-order accurate in time, but does not significantly reduce the overall accuracy since it is only used roughly once every 25 steps.

3. Examples of model results

Some results of integrations over a range of scales of topography are presented in this section. Parameters were chosen so that the flows bear some resemblance to atmospheric flows. The fluid viscosity, ν_0 is $5 m^2 s^{-1}$, and the Coriolis parameter, f, is 10^{-4} s^{-1}, giving an Ekman boundary layer depth $\delta = \left(\frac{2\nu_0}{f}\right)^{\frac{1}{2}}$ of approximately 300m. $\frac{dP_0}{dy}$ is chosen to give a geostrophic wind $U_0 = -\frac{1}{f}\frac{dP_0}{dy}$ of 10 ms^{-1}. The first two examples are of homogeneous flow, ie contain no buoyancy effects.

In order to provide some verification of the method of representation of topography we first present a comparison with a linearised analytic theory. The theory is based on a 'triple deck' analysis of the type discussed by Smith [11] and is described in detail in Sykes [12]. This is an asymptotic theory based on the small parameter $(\nu_0/U_0\delta)^{\frac{1}{4}}$ which for the present case has a value of 0.22. The theory has been linearised by assuming the height of the hill is small, and

the small parameter involved in this is 0.2. Figure 4 shows the dimensionless surface pressure from the theory compared with the model results, and it is clear that the errors are well within the limits of accuracy expected of the theory ie $\sim 20\%$.

The next example is that of strongly separated flow past an obstacle 50 m high with slopes of order 45°. For this case the only relevant scale is λ (see § 2a) which is ~ 25m giving $\frac{\Delta}{\lambda} \sim \frac{1}{4}$. Figure 5(a) shows contours of the streamfunction, contour values being chosen to give a fairly uniform spacing on the stretched grid. The solution presented is close to equilibrium and is characterised by a long separation bubble. The pressure field is shown in figure 5(b), and it can be seen that the pressure varies smoothly across the surface of the obstacle. Along the surface there is a strong favourable pressure gradient associated with the acceleration of fluid over the obstacle, but due to the separation behind the obstacle, the corresponding adverse pressure gradient is greatly reduced.

Although not particularly evident in Figure 5, we should emphasise that the contour plotting program is simply based on linear interpolation between grid-point values. Since the plotting program has no information about the interpolated viscosities, this procedure can produce spurious contours near the surface. These effects are more obvious in figure 6.

The final example includes effects due to a stable stratification which are, of course, important in many geophysical flows. In the simulation of such flows it is normal to use a form of radiation boundary condition at the upper boundary to allow gravity wave energy to leave the domain of integration. The use of such boundary conditions is independent of the method of representing topography, and in this example a radiation condition at $z = H$ was simulated by the use of Rayleigh damping on the uppermost 5 grid points (for details and other examples see Mason and Sykes [13]).

The basic stratification is chosen such that the Brunt-Vaisala frequency $N = \left[\frac{g}{\rho}\frac{d\rho}{dz}\right]^{\frac{1}{2}} = 10^{-2}\,s^{-1}$ and to prevent the generation of 'slope winds', due to temperature contrast between the hill and the adjacent fluid, the densities beneath the surface are taken to correspond to the basic stratification.

Figure 6 shows steady flow over a long length-scale hill which is higher than the boundary layer. The hill is 1 km high and 60 km long in a periodic domain of length 240 km and depth 15 km. In this case the scale λ is ~ 200 m giving $\frac{\Delta}{\lambda} \sim \frac{1}{3}$, whilst the stratification length scale is some $2\frac{1}{2}$ times greater than λ and consequently unimportant. Figures 6(a, b) show the u-and w-components of velocity, respectively. On this length-scale, the principal effects in u and w are due to the strong stratification. This inhibits vertical motions, forcing the fluid to rise gently upstream and flow over the summit in a vertically constricted jet. On the leeward slope, the buoyancy forces rapidly accelerate the fluid as it returns to its equilibrium level. Note that the buoyancy forces have made the flow separation nearly symmetric about the centre of the hill.

Figure 6c shows the buoyancy perturbation from the undisturbed state; as with the u and w fields, vertically propagating gravity waves are evident. Finally figure 6d shows the pressure field; it can be seen that since the slope of the topography is small, $\frac{\partial f}{\partial z}$ is almost zero at the surface.

4. Conclusions

When the viscous boundary layer resolution requirements discussed in § 2a are met, it is possible to include topography into a Cartesian model without loss of accuracy. The method can be considered in two parts :

1. Small terms are neglected near the surface.
2. The diagnostic Poisson equation for pressure is solved in the entire rectangular domain by posing a trivial physical model for the state of zero motion beneath the surface. Motivation for using this method, in problems where the resolution requirements can be accomodated, lies in the ease of adaptation of an existing Cartesian code and the fast execution speed in comparison with more formally accurate methods. The examples given here and in Mason and Sykes [13] demonstrate the utility of the method.

Acknowledgement

The authors gratefully acknowledge the work done by Dr L Farnell in the development of the basic Cartesian code used in the present work.

REFERENCES

1. Gal-Chen, T. & Somerville, R C J, J.Comp.Phys (1975) 17 pp. 209-228
2. Gal-Chen, T. & Somerville, R C J., J.Comp.Phys. (1975) 17 pp. 276-310
3. Thompson, J.F., Thames F C, Hodge, J K., Shanks, S P., Reddy, R N and Mastin, C W, Lecture Notes in Physics (1976), 59 pp. 421-428.
4. Hirt, C W, Amsden, A A., & Cook, J L., J.Comp.Phys (1974) 14 pp. 227-253
5. Pracht, W E., J.Comp.Phys (1975) 17 pp. 132-159
6. Roache, P J 'Computational Fluid Dynamics' Hermosa Publishers, Albuquerque (197
7. Stewartson, K., Advances in Appl. Mechs. (1974) 14 p. 145 - 239
8. Williams, G P., J. Fluid Mech. (1969) 37 pp. 727-750.
9. Piacsek, S A & Williams, G P., J.Comp.Phys.(1970) 6 pp. 392-405
10. Lipps, F B., J.Comp.Phys. (1977) in Press
11. Smith, F T., J. Fluid Mech. (1973) 57 pp. 803-824.
12. Sykes, R I in preparation.
13. Mason, P J and Sykes, R I submitted to Quart.J.Roy.Met.Soc. (1977).

Legends

Figure 1.

Schematic diagram of domain of integration.

Figure 2.

Illustrating the intersection of the surface S and a vertical line of grid points.

Figure 3.

The staggered mesh.

Figure 4.

A comparison of dimensionless surface pressure p^* between the numerical model and analytic theory. The hill has the form $z = \cos^2(\pi x)$, $/x/ \leq 0.5$ and $z = 0$ otherwise. The smooth curve is from the theory and the values of p^* at grid points are indicated by the open circles.

Figure 5.

Numerical results obtained with a mesh of 64 by 24 points. The results are presented with a uniform spacing between grid points, the actual grid point heights in metres are indicated on the right hand side of the diagram.

(a) shows streamlines, chosen to give an almost uniform spacing in the absence of topography.

(b) shows the corresponding pressure field. The contour interval is 0.125 Nm^{-2} and negative values are denoted by dashed lines. The zero contour is shown as a slightly heavier solid line. These plotting conventions apply to Figure 6.

Figure 6.

Numerical results obtained with a mesh of 64 by 36 points.

(a) shows the x-component of velocity u plotted with a contour interval of $1.0\ ms^{-1}$.

(b) shows the vertical component of velocity w plotted with a contour interval of $5.5 \times 10^{-2}\ ms^{-1}$.

(c) shows buoyancy ($-\frac{g\rho}{\bar{\rho}}$) perturbations from the initial state plotted with a contour interval of 6.0×10^{-3} ms^{-2}.

(d) shows the pressure field plotted with a contour interval of 8.3 Nm^{-2}.

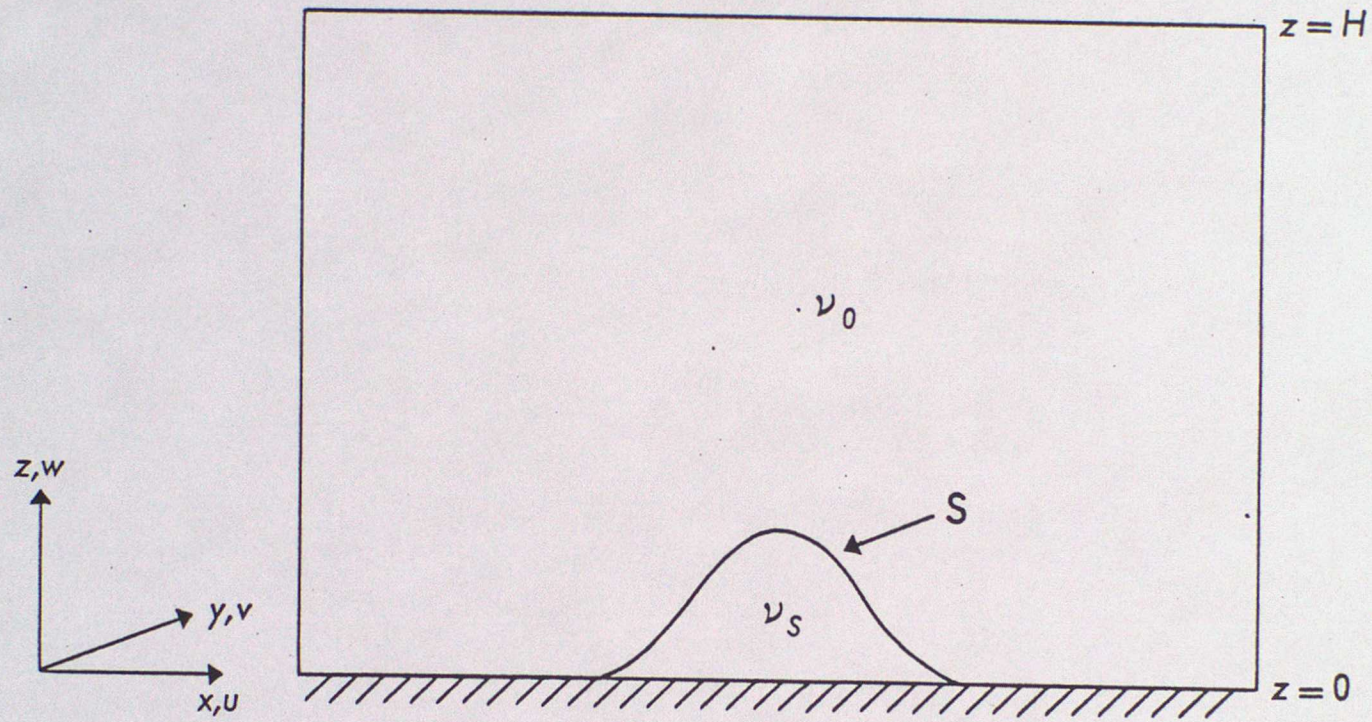

Figure 1

J. Comp. Phys.
Mason & Sykes

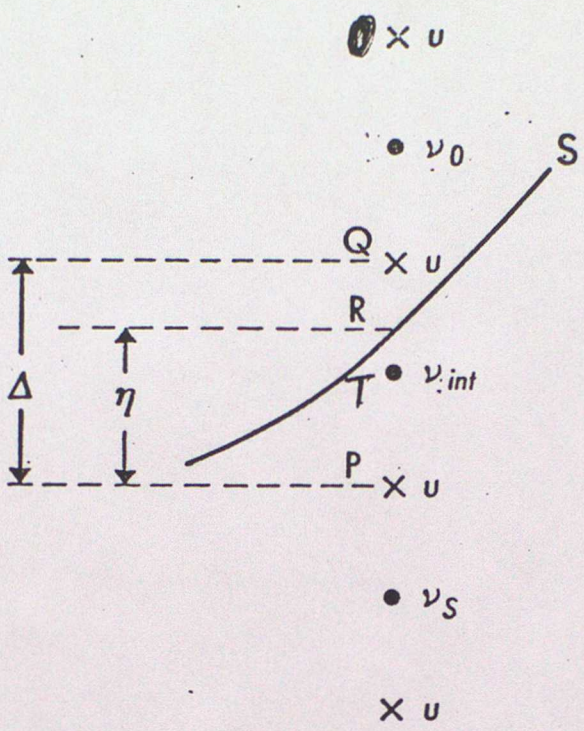

Figure 2

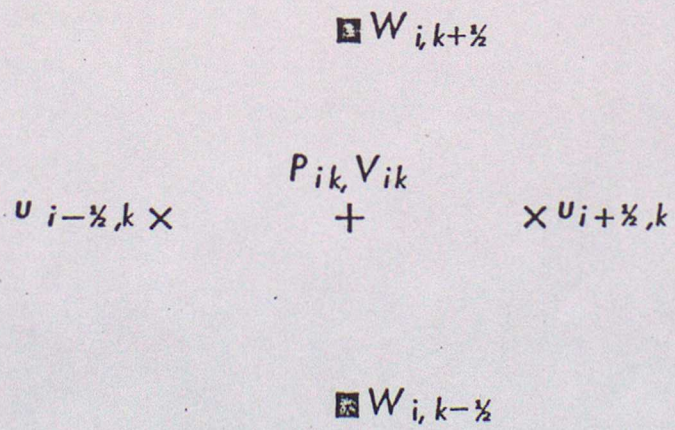

Figure 3

J. Comp. Phys.
Mason & Sykes

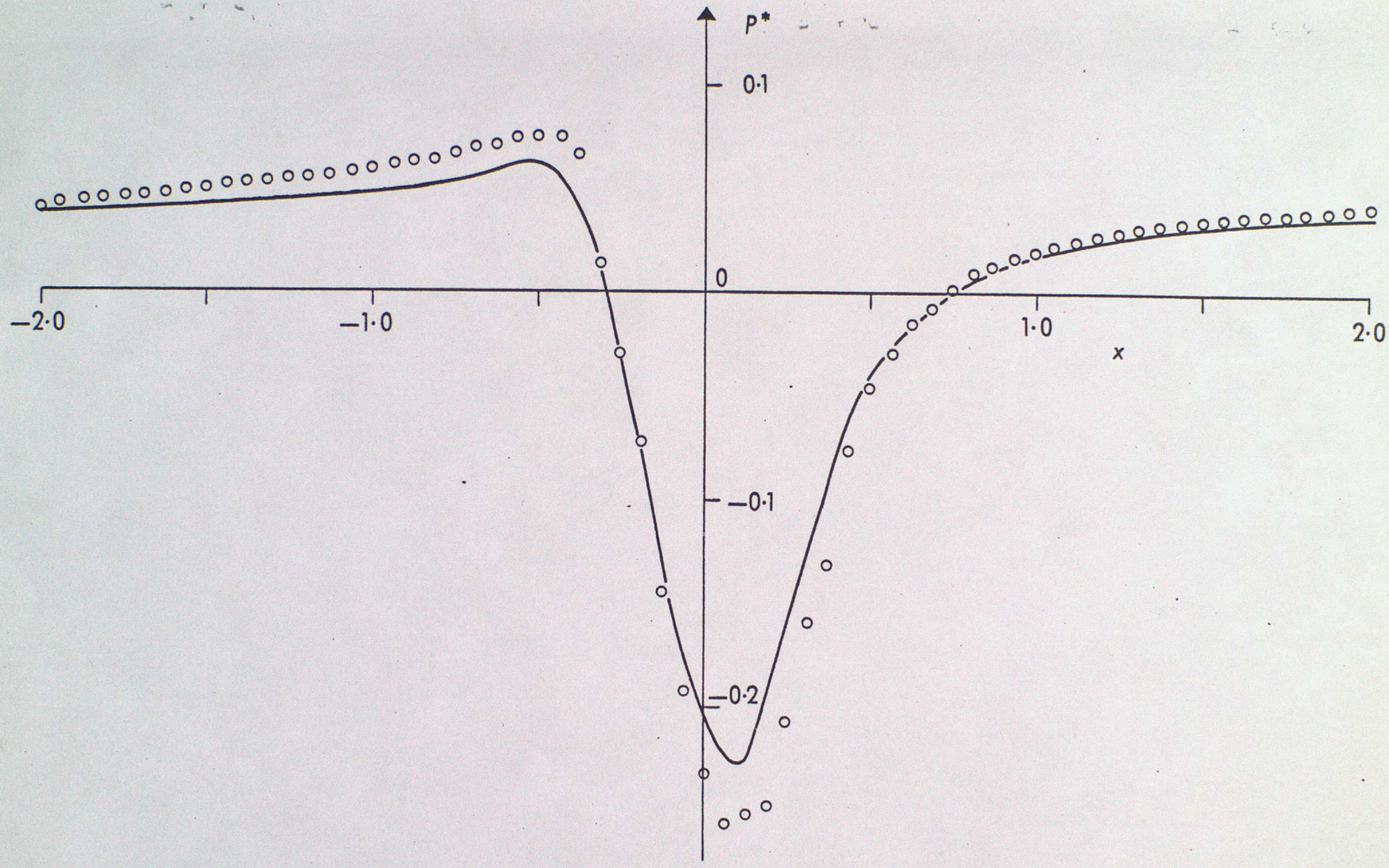

J. Comp. Phys.
Mason & Sykes

Figure 4

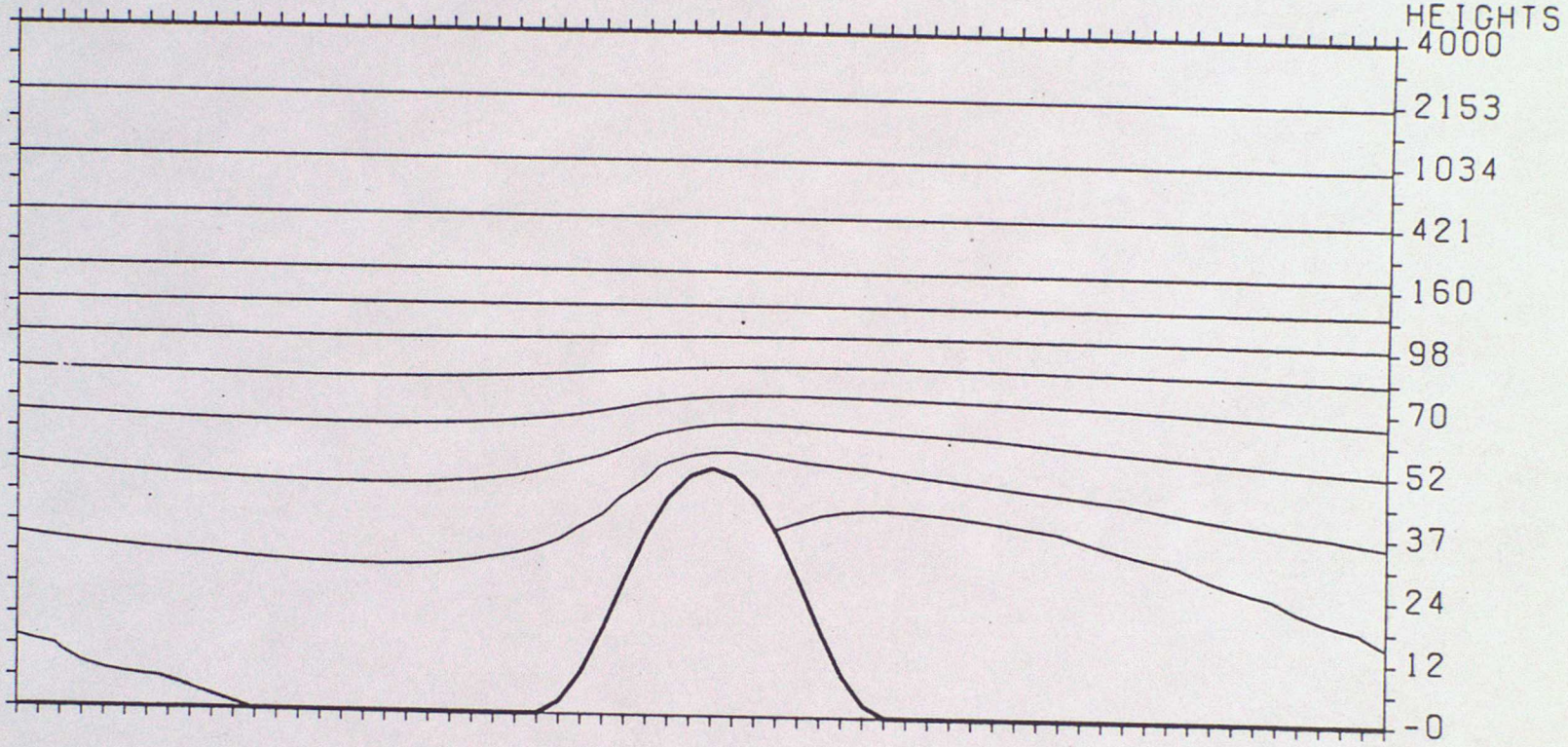

Fig 5a

J. Comp. Phys.
Mason & Sykes

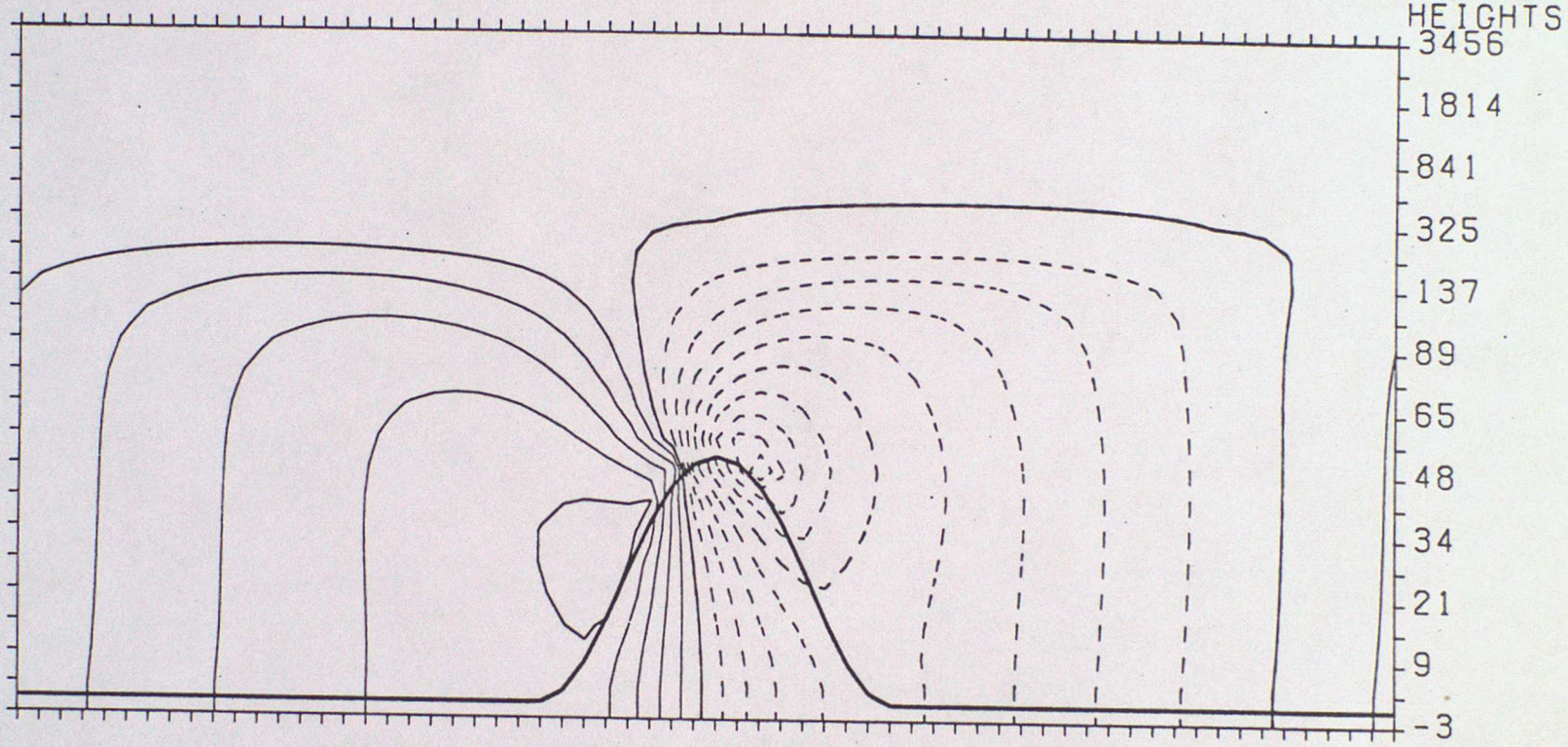

J. Comp. Phys.
Mason & Sykes

Fig 5 b

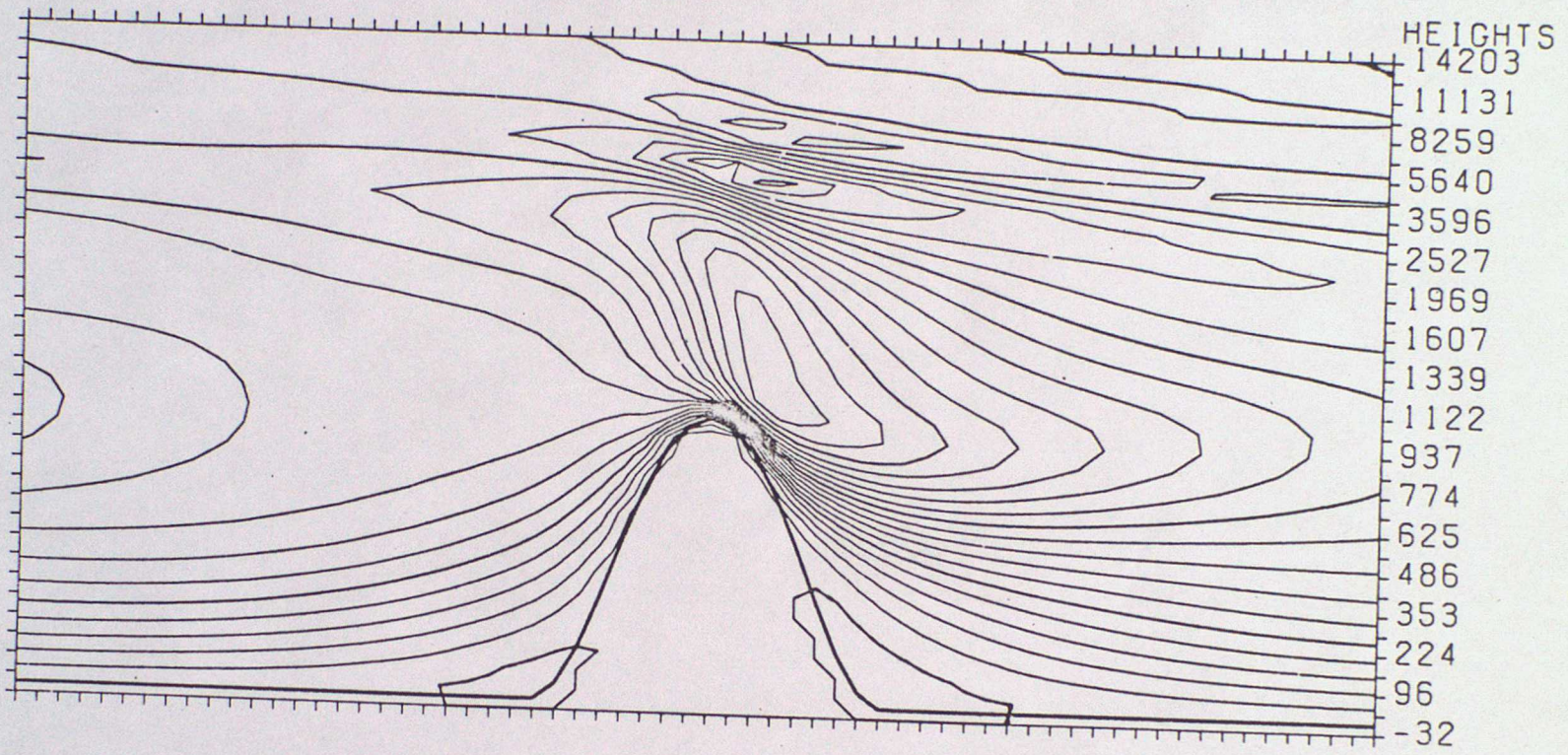

J. Comp. Phys.
Mason & Sykes

Fig. 6a

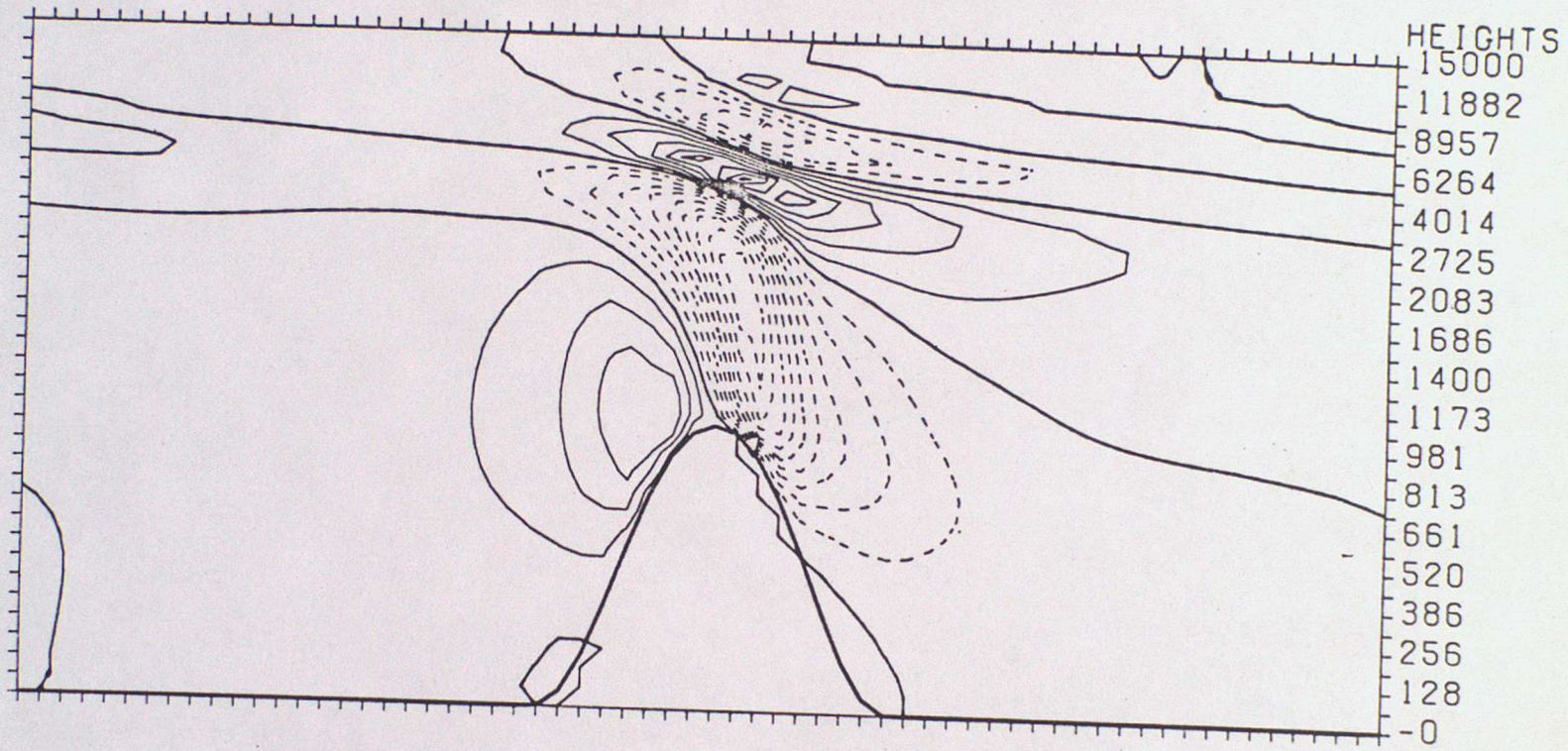

J. Comp. Phys.
Mason & Sykes

Fig 6b

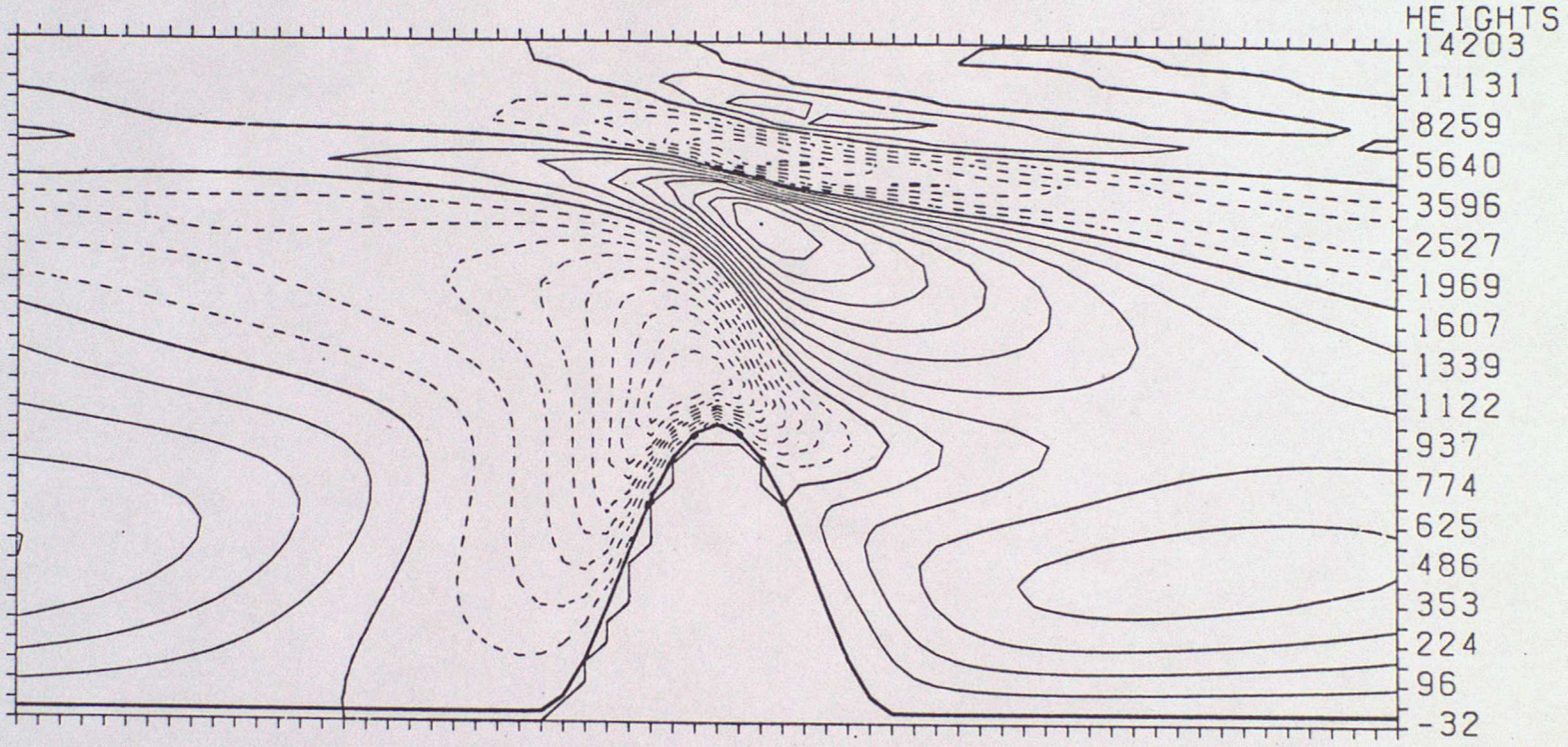

J. Comp. Phys.
Mason & Sykes

Fig 6c

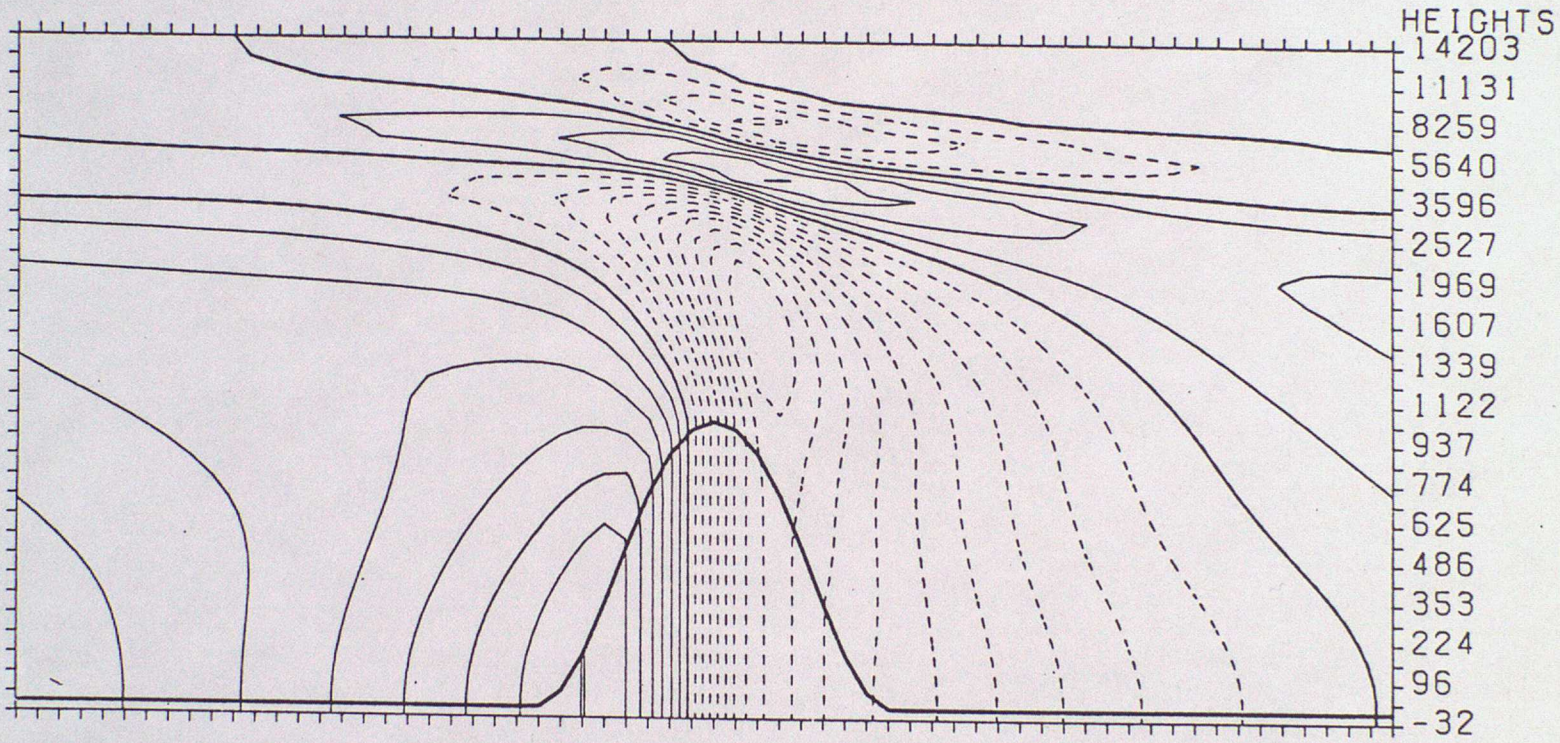

Fig. 6d

J. Comp. Phys.
Mason & Sykes